# Winter equatorial mesospheric neutral turbulence

**Uma Das[1,2,*] and H. S. S. Sinha[1]**

[1]Space and Atmospheric Sciences Division, Physical Research Laboratory, Navrangpura, Ahmedabad 380 009, India
[2]Present address: Institute of Space Science, National Central University, Jhongli 320001, Taiwan

**A Rohini sounding rocket carrying a Langmuir probe was flown from Thumba (8.3°N, 76.9°E), India on 27 November 2005 to study the winter equatorial mesospheric neutral turbulence from electron density measurements. The most important result of this study is the detection of a few thin intermittent turbulent layers of 100–200 m thickness, and this was possible due to the use of the continuous wavelet transform technique. This study shows that the winter turbulence is very weak. Also, the contribution of neutral turbulence process towards heating the mesosphere is significantly less during winter.**

**Keywords:** Continuous wavelet transform, mesosphere, turbulence.

NEUTRAL turbulence plays a major role in the energy budget of the mesosphere. It is an important heating source in this part of the atmosphere especially during summer[1,2]. Gravity waves produced in the lower atmosphere propagate upward and eventually break at these altitudes producing turbulence and depositing energy and momentum. The energy at the large scales cascades down to intermediate and then to smaller scales where it is finally lost by viscous dissipation, maintaining the energy balance. The energy cascade process follows the Kolmogorov's –5/3 power law and the viscous dissipation process follows a –7 power law. The inner scale is the breakpoint where the spectral slope changes from –5/3 to –7.

The mesosphere is a weakly-ionized, collision-dominated region and hence controlled by neutral dynamics. Any neutral turbulence is therefore transferred to the electrons and ions in this region[3]. Mesospheric neutral turbulence can be studied *in situ* using rocket-borne measurements of electron/ion density fluctuations[1,2,4,5], using electrons/ions as passive tracers. The electron and ion concentrations do not change through ion production, recombination or chemical reactions within the characteristic lifetime of an eddy and hence are efficient tracers of neutral turbulence in the mesosphere, i.e. at heights below ~90 km. Mesospheric turbulence is also seen in very high frequency (VHF) radar signal-to-noise ratio (SNR) maps as strong backscattered echoes from regions of electron density irregularities[5–8]. Turbulence parameters, viz. the energy dissipation rate and heating rate can be estimated from these measurements.

*For correspondence. (e-mail: umakota@gmail.com)

Using simultaneous rocket-borne measurements of electron densities and mesosphere stratosphere troposphere (MST) radar observations during summer, turbulent parameters were estimated over low latitudes[2,5]. These studies show that the mesospheric turbulence during summer is strong and the energy dissipation rates estimated by Chandra *et al.*[5] using rocket observations ranged between 1 and 200 mW/kg and that with the radar observations was around 23 mW/kg. So far, there have been no rocket-borne investigations of the mesospheric turbulence during winter over the Indian low and equatorial latitudes and therefore in the present work rocket-borne electron density measurements are used to study the mesospheric neutral turbulence over equatorial latitudes during winter. The summer–winter differences and similarities in turbulence parameters are also addressed in this study.

The spectral analysis technique used in earlier studies was mostly the Fourier transform or the short-time Fourier transform, which required a sufficiently long length of data of approximately 1 km. The altitude resolution of the turbulence parameters thus estimated was of the same order. Recent advances in mathematical tools have seen the growth of the continuous wavelet transform (CWT) which has become a powerful tool to understand the geophysical phenomena in both the frequency and the time (here altitude) domains, simultaneously. In the present study, CWT has been used and it has improved the altitude resolution of the turbulence parameters tremendously and enabled the understanding of the fine structures in the mesospheric turbulence[2].

A Rohini sounding rocket, RH-300 MK II, carrying an ogive-shaped Langmuir probe (LP) was launched during daytime to study the equatorial mesosphere and lower thermosphere. The flight was launched from Thumba (8.3°N, 76.9°E) on 27 November 2005 at 11:23 h LT (UT + 5.5 h). The rocket reached an apogee of 109 km and covered a horizontal range of 125 km. The spin frequency of the rocket during this flight was 8.5 per sec. The LP sensor was placed along the spin axis of the rocket to measure electron density fluctuations. The LP sensor was biased at +4 V and was mounted at the rocket nose tip. The electrical connection to the signal conditioning electronics was provided by means of a coaxial cable. The electronics was accommodated in a package mounted on one of the instrument decks. To cover the large dynamical range, arising from the change in current due to variation in the electron density, an automatic gain amplifier was used to measure the current in the range of 1 nA to about 3 μA. For studying the electron density fluctuations in different scale sizes, the current collected by the LP sensor was processed onboard in three channels with different gains having frequency response of 0–100, 30–150 and 70–1000 Hz, which are named as LP main, LP medium frequency (MF) and LP high frequency (HF) channels respectively. Information regarding various scale sizes ranging from a kilometre to less than a metre

was obtained from these three channels. Other specifications of the Langmuir probe experiment were similar to those given by Prakash and Subbaraya[9].

The geophysical conditions on the day of flight were quiet with a daily $A_p$ value of 3 and $K_p$ index of 5+. The F10.7 cm solar flux was $78 \times 10^{-22}$ Wm$^{-2}$.

The analysis of data from the rocket flight was done using the CWT, similar to the procedure described in Das *et al.*[2]. A complete description of the CWT is given in literature[10,11] and is briefly described here.

The wavelet transform, relative to some basic wavelet, provides a flexible time frequency window which automatically narrows when observing HF components and widens when observing low frequency components. The technique of using wavelets to identify localized power events in time series is now being used and applied in various studies starting from stock market fluctuations to geophysical phenomena. Relative to every basic wavelet $\psi$, that satisfies the 'admissibility' condition,

$$\int_{-\infty}^{\infty} \psi(t)\mathrm{d}t = 0, \tag{1}$$

CWT, $W_x^{\psi}(s, \tau)$, of a function $x(t)$ is defined as

$$W_x^{\psi}(s,\tau) = \frac{1}{\sqrt{|s|}} \int_t x(t)\, \psi^*\left(\frac{t-\tau}{s}\right)\mathrm{d}t. \tag{2}$$

The transformed signal, $W_x^{\psi}(s, \tau)$, is a function of two variables, $s$ and $\tau$, i.e. scale and translation. These two parameters correspond to frequency and time respectively. $\psi((t - \tau)/s)$ is called the mother wavelet and $\psi^*((t - \tau)/s)$ is its conjugate. It is so called because all the wavelets to be used in the analysis are derived from this function. The factor $1/\sqrt{|s|}$ is for energy normalization.

For a discrete equally spaced time series $x_n$ (like in the dataset used in the present study), where $n = 0, 1, \ldots, N-1$ is the index in time, the convolution of $x_n$ with a scaled and translated version of $\psi$ gives the continuous wavelet transform[9]:

$$W_n(s) = \sum_{n'=0}^{N-1} x_{n'} \psi^*\left[\frac{(n'-n)\delta t}{s}\right]. \tag{3}$$

By varying the wavelet scale $s$ and translating along the localized time index $n$, the wavelet coefficients can be computed. The wavelet transform $W_n(s)$ is real ($R\{W_n(s)\}$) or complex ($R\{W_n(s)\}$) + i($I\{W_n(s)\}$) depending on whether the wavelet function $\psi$ is real or complex respectively. The wavelet power spectrum can thus be defined as $|W_n(s)|^2$. The software written in IDL provided by Torrence and Compo[11] was used for the present analysis. The morlet wavelet, which is a plane wave modulated by a Gaussian was used for computing the wavelet coefficients. It is a complex wavelet and is given as:

$$\psi_0(\eta) = \pi^{-1/4} \mathrm{e}^{\mathrm{i}\omega_0\eta} \mathrm{e}^{-\eta^2/2}, \tag{4}$$

where $\eta$ is a dimensionless time parameter and $\omega_0$ the frequency, here taken to be 6 to satisfy the admissibility condition.

The current collected by the LP sensor in the main channel was converted into electron density using a conversion factor of 1740 electrons cm$^{-3}$ $\mu$A$^{-1}$ from earlier calibration studies[12]. CWT was then used to compute the power spectra of the electron density from the main channel and also of the fluctuations in the other two AC (MF and HF) channels. The power spectra corresponding to an altitude region of 100 m were averaged for all three channels and the MF and the HF channel spectra were then normalized to that of the main channel at 50 and 100 Hz respectively to make composite spectra in the frequency range of DC–1000 Hz (ref. 2). A range of 100 m was chosen to make sure that the breakpoints observed in the spectra are indeed present in the data set. Secondly, averaging the spectra over 100 m assures that consecutive spectra contain independent information on the relevant spatial scales between 10 and 100 m. Finally, the other reason for this choice is to ensure numerical stability of the fitting algorithm[13].

The well-known Heisenberg model with a smooth transition from the Kolmogorov's –5/3 slope in the inertial subrange to the steeper viscous dissipation regime with a slope –7 was used to identify the innerscale, $l_0$, of turbulence. Turbulence is presumed to be present only at those altitudes where the observed spectra fitted well with the Heisenberg model spectra and hence turbulence parameters were computed only at these altitudes. The turbulent parameters have then been estimated using the usual procedures[2,5,14,15]. The Kolmogorov scale $\eta$, which is the smallest scale at which an eddy can exist, is given by[16]

$$\eta = \frac{l_0}{7.4}. \tag{5}$$

The energy dissipation rate is given by[17,18],

$$\varepsilon = \frac{\nu^3}{\eta^4}, \tag{6}$$

where $\nu$ is the kinematic viscosity computed from the MSISE-90 model[19] temperatures and densities. The heating rate is then given by[1]

$$\frac{\delta T}{\delta t} = \frac{\varepsilon}{C_P} = 0.0864\varepsilon \ (K/\mathrm{day}), \tag{7}$$

where $C_P$ = 1003 J/(K kg) is the specific heat of air at constant pressure, given $\varepsilon$ in mW/kg.

Figure 1 shows the electron density measured during the ascent of the rocket flight during winter on 27

November 2005 (thick blue solid line). The densities measured during the earlier summer flight (thin red solid line) from Sriharikota[5] are also shown for comparison. Electron density profiles from both flights were largely similar in shape and number densities. During the present winter flight, a maximum density of $\sim 2 \times 10^5$ cm$^{-3}$ was observed over a wide region of 100–110 km, unlike the sharp peak seen during the summer flight at 98 km. The typical E-region ledge is seen very prominently at 87 km during the present winter flight. Electron densities from the IRI2001 model, for the launch conditions of both the flights (dashed lines), are also shown in the figure. Model results for both flights are similar to each other. Below 87 km, the model underestimates the observed densities and above these altitudes it matches quite well with the measurements. In order to show the presence of steep gradients, variation of the inverse of the electron density gradient scale length, $L^{-1}[1/L = (1/n_e)(dn_e/dh)]$ was studied. A larger $L^{-1}$ indicates steeper electron density gradient. Very strong positive and negative electron density gradients were present in both flights. Figure 2 shows the variation of $L^{-1}$ during the winter flight. Strong gradients were present in the altitude region of 87–99 km and very strong gradients were present in the E-region ledge from 87 to 89 km.

Figure 3 shows the results obtained by subjecting the electron density data to the continuous wavelet transform. The left panel of the figure shows the high resolution electron density data obtained from the LP main channel that was used for the computation of the wavelet coefficients. The right panel shows the wavelet power spectra computed from data in LP main, MF and HF channels, spanning the complete frequency range from DC to 1000 Hz. The contour is a composite of all the altitude-averaged power spectra (computed according to the procedure described earlier), and normalized with the square of the electron density, so that the power spectra are comparable at all altitudes. The white long-dashed lines in Figure 3 show the change in frequency with altitude for various scale sizes. As the vertical velocity of the rocket decreases with altitude, the frequency at which these scale sizes appear decreases accordingly resulting in the bend in these lines towards the lower frequencies. The vertical black line shows the spin frequency (8.5 s$^{-1}$) of the rocket. As LP sensor was placed along the spin axis of the rocket, the effect of spin was very small and is seen only above 100 km, when the rocket was approaching the apogee.

Each of the altitude-averaged power spectra was verified for the characteristic –5/3 Kolmogorov scale of the inertial subrange and the viscous dissipation regime of –7 slope. Figure 4 shows three examples of consecutive spectra at altitudes 71.8–72.0, 80.4–80.6 and 84.5–84.7 km. For the spectra where the Heisenberg model could be fitted, the model is shown in red. Slopes of –5/3 and –7 are also plotted to appreciate the model fit, which shows the presence of turbulence at these altitudes. The inner scale $l_0$ identified from the fit is denoted by a vertical dashed line in each of these spectra. For the spectra where the model could not be fitted, the spectral indices are found from linear fits (shown in blue) to show that they are indeed different from –5/3 and the –7 slope does not exist at all, thereby showing that at these altitudes there was no turbulence. The first set of spectra in the top row show an example of a single turbulent layer of 100 m thickness at 71.9 km sandwiched between two layers

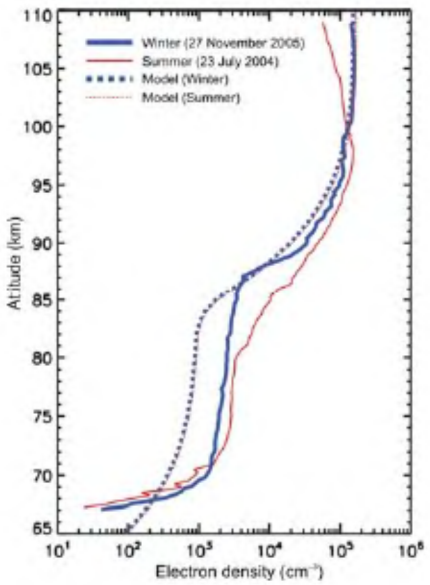


**Figure 1.** Electron density measured by the Langmuir probe during the ascent of the rocket flights during winter (thick blue solid line) at 100 m resolution. Observations from the previous summer flight (thin red solid line)[5] and IRI2001 model profiles (dashed lines) for the rocket launch conditions of both flights are also shown for comparison.

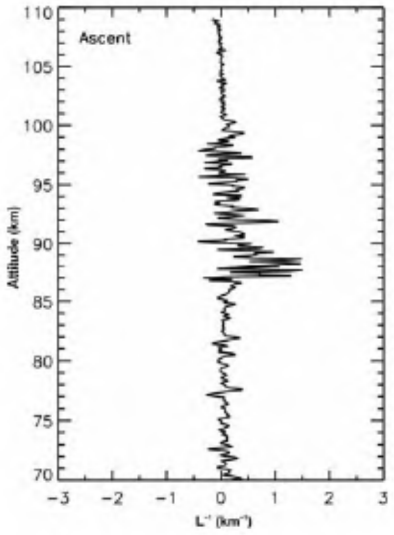


**Figure 2.** Variation of inverse of electron density gradient scale length ($L^{-1}$) with altitude during the rocket ascent for the winter flight (27 November 2005). Very steep gradients are present in 87–99 km region.

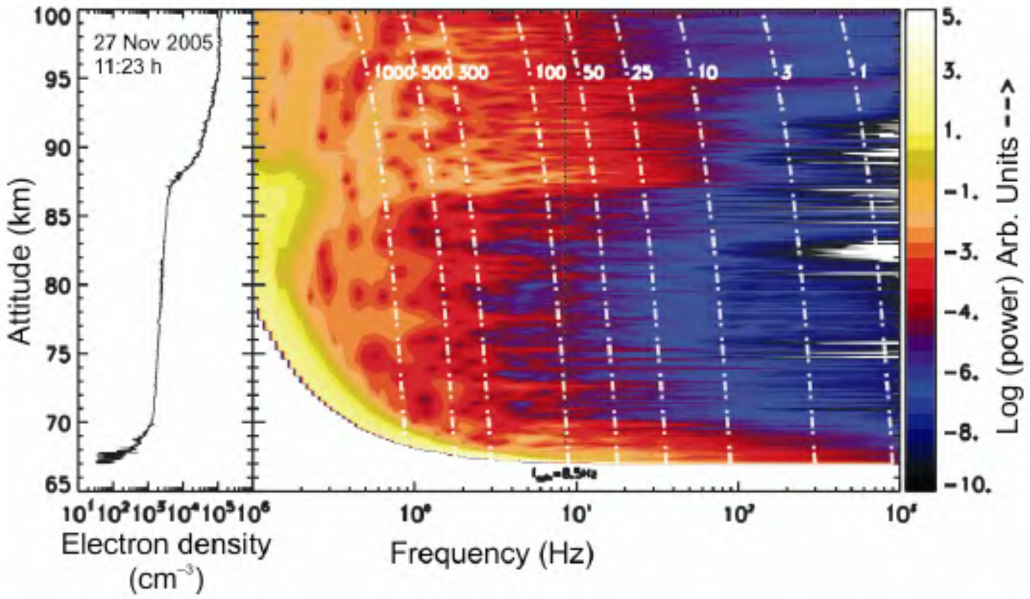


**Figure 3.** The left panel shows the high-resolution electron density data obtained from the Langmuir probe main channel during the winter flight. The right panel shows the composite of all altitude-averaged wavelet power spectra normalized with the average electron density. See text for more details.

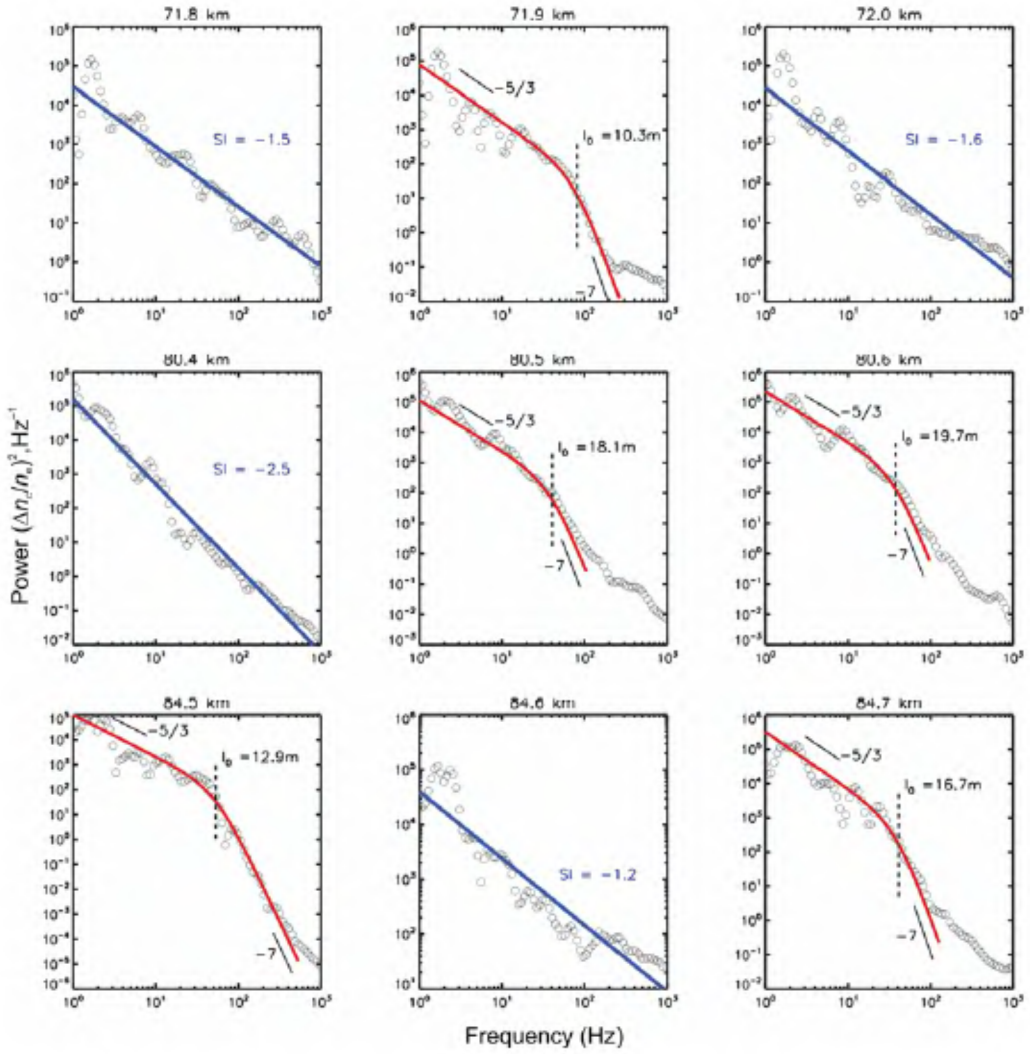


**Figure 4.** Three sets of consecutive altitude-averaged power spectra in 100 m bins around 71.9, 80.5 and 84.6 km during the winter flight. See text for more details.

(71.8 and 72.0 km) where no turbulence is observed. In the second row, it can be seen that two consecutive spectra show characteristics of turbulence. And in the last row, it can be observed that there are two regions of turbulence at 84.5 and 84.7 km which are sandwiching a layer devoid of turbulence. All these spectra show the intermittency that can exist in turbulent layers in the mesosphere region.

Figure 5 shows the inner scales identified from all spectra for which the Heisenberg model could be fitted. The inner scale varied between 10 and 45 m with a mean of 20 m. This figure shows the existence of thin layers for turbulence of thickness 100 m. The intermittency at which these turbulent layers can exist is also seen. This is in contrast to the near continuous turbulent layers observed during the earlier summer flight[2]. Figure 6 shows the energy dissipation rates and the heating rates estimated from all these spectra that showed turbulence characteristics for the winter flight (blue triangles). Results from the earlier summer flight[2] (red circles) and an earlier study from India[14] (black stars) and the high latitude winter (solid blue line) and summer (dashed red line) averages[1] are also shown in the figure for comparison. The energy dissipation rates during winter at lower altitudes (70–78 km, hereafter called region I) ranged from 0.1 to 6 W/kg and the corresponding heating rates ranged from 0.01 to 0.6 K/day. In the higher altitudes (83–87 km, hereafter called region II), the energy dissipation rates ranged from 10 to 1000 mW/kg and the heating rates ranged from 1 to 100 K/day. In and above the E-region ledge above 87 km (region III), which has sharp vertical electron density gradients, many altitude-averaged power spectra (not shown here) could be fitted with the Heisenberg model. However, in view of the fact that the electron density gradients are very large, plasma instabilities like gradient drift instability will operate in this region. Therefore, the contribution of neutral turbulence cannot be estimated and hence this region is not further investigated.

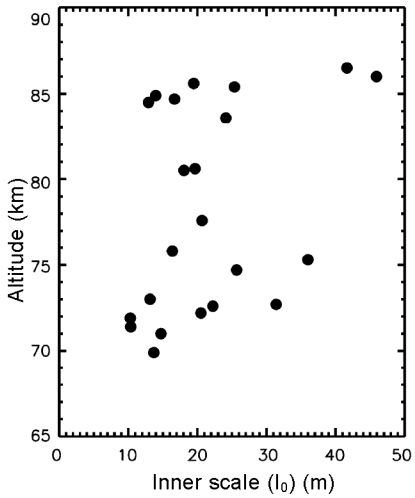


**Figure 5.** Variation of inner scale of turbulence ($l_0$) with altitude at 1123 h. Local time obtained from the rocket flight conducted from Thumba on 27 November 2005.

The high latitude summer energy dissipation rates[1] range from 1 to 156 mW/kg (the corresponding heating rates range from 0.1 to 14 K/day) in 79–97 km, with a peak at around 90 km. During winter, turbulence is observed in the entire mesosphere from 60 to 100 km but values are much smaller, ranging from 1 to 20 mW/kg (the corresponding heating rates range from 0.1 to 1–2 K/day). In the present study, the observed winter turbulence in region I is similar to the high-latitude winter average. However, in region II, the observed winter turbulence is much stronger than the high-latitude winter average and is similar to that observed during summer at both, low- and high-latitudes.

The most important result obtained from these rocket-borne measurements is the detection of thin intermittent layers of turbulence with thickness as small as 100 m. Although thin turbulent layers have been seen earlier[2,13] and were also predicted by direct numerical simulation studies[20], the results are interesting due to the intermittency of these layers. This suggests that the winter turbulence is very weak and can be identified in the data only with the help of mathematical tools like the continuous wavelet transform. These could not have been observed with traditional methods like Fourier transform.

Turbulence in the mesospheric altitudes is generated mainly through breaking of gravity waves[20]. The gravity waves are produced in the lower atmosphere and propagate upward carrying energy and momentum. As they

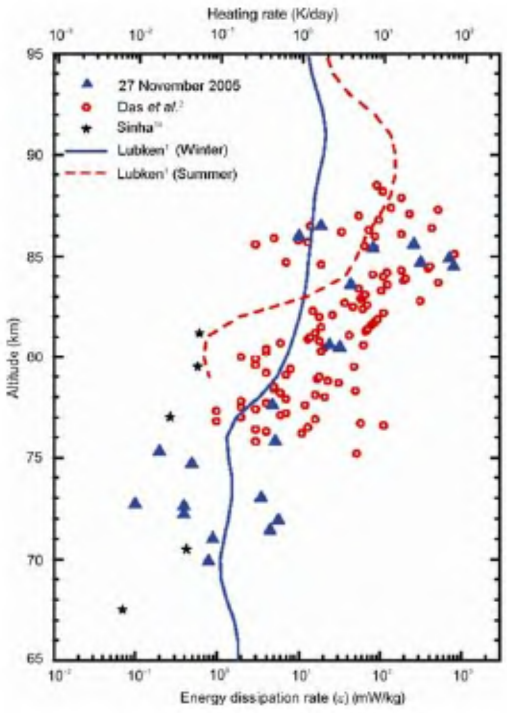


**Figure 6.** Energy dissipation rates and the corresponding heating rates during winter (blue triangles). Results from the earlier summer flight[2] (red circles) and previous study from India[14] (black stars) and the high latitude winter (solid blue line) and summer (dashed red line) averages[1] are also shown in the figure for comparison.

propagate, their amplitude increases due to decreasing atmospheric density and at mesospheric altitudes they break depositing the energy and momentum carried from lower regions. Satellite studies have shown that the gravity wave activity is strong over the Indian low and equatorial latitudes during summer and is weak during winter[21]. This is in conformity with the present results where the observed turbulence in the winter mesosphere over the equator is very weak. It has been shown earlier that during summer strong gravity wave activity produces strong turbulence[2]. Though the estimated energy dissipation rates are higher in the present study, especially in region II, the observed turbulence is very intermittent, i.e. occurs in only few thin layers. It is therefore inferred that the contribution of the turbulence process towards heating of the mesosphere during winter is significantly less.

High-latitude studies also showed that the contribution of neutral turbulence to the heating of the winter mesosphere is significantly less[22]. However, the energy dissipation rates and the heating rates that were estimated were also significantly less. Whereas in the present study, the energy dissipation rates and heating rates that are observed in the mesosphere are high and comparable to summer values. However, as they are present in thin layers, it is inferred that the contribution of turbulence towards heating the winter mesosphere is less. And we could arrive at these results, due to the identification of the thin layers of turbulence by using the CWT technique.

Using electrons as tracers, the mesospheric neutral turbulence has been studied and the continuous wavelet transform was used for the spectral analysis. The most important result of this study is the identification of a few thin intermittent turbulent layers of 100–200 m thickness. In lower altitudes (70–78 km, region I) heating rates are similar to earlier winter studies, whereas at high altitudes (80–87 km, region II), they are higher and comparable to summer values. However, because they occur in thin layers, the contribution of turbulence towards heating of the winter equatorial mesosphere is significantly less in comparison to that of summer.


1. Lübken, F. J., Seasonal variation of turbulent energy dissipation rates at high latitudes as determined by *in situ* measurements of neutral density fluctuations. *J. Geophys. Res.*, 1997, **102**, 13441–13456.
2. Das, U., Sinha, H. S. S., Sarma, S., Chandra, H. and Das, S. K., Fine structure of the low latitude mesospheric turbulence. *J. Geophys. Res.*, 2009, **114**, D10111.
3. Thrane, E. V. and Grandal, B., Observations of the fine scale structure in the mesosphere and lower thermosphere. *J. Atmos. Terr. Phys.*, 1981, **43**, 179–189.
4. Lehmacher, G. A., Goldberg, R. A., Schmidlin, F. J., Croskey, C. L., Mitchell, J. D. and Swartz, W. E., Electron density fluctuations in the equatorial mesosphere: neutral turbulence or plasma instabilities. *Geophys. Res. Lett.*, 1997, **24**, 1715–1718.
5. Chandra, H. *et al.*, First mesospheric turbulence study made using coordinated rocket and MST radar measurements over Indian low latitude region. *Ann. Geophys.*, 2008, **26**, 2725–2738.
6. Chakravarty, S. C., Datta, J., Kamala, S. and Gupta, S. P., High resolution mesospheric layer structures from MST radar backscatter echoes over low latitude. *J. Atmos. Sol. Terr. Phys.*, 2004, **66**, 859–866.
7. Kamala, S., Narayana Rao, D., Chakravarty, S. C., Datta, J. and Prasad, B. S. N., Vertical structure of mesospheric echoes from the Indian MST radar. *J. Atmos. Sol. Terr. Phys.*, 2003, **65**, 71–83.
8. Sheth, R. *et al.*, A high-resolution study of mesospheric fine structure with the Jicamarca MST radar. *Ann. Geophys.*, 2006, **24**, 1281–1293.
9. Prakash, S. and Subbaraya, B. H., Langmuir probe for the measurement of electron density and electron temperature in the ionosphere. *Rev. Sci. Instrum.*, 1967, **38**, 1132–1136.
10. Farge, M., Wavelet transforms and their applications to turbulence. *Annu. Rev. Fluid Mech.*, 1992, **24**, 395–457.
11. Torrence, C. and Compo, G. P., A practical guide to wavelet analysis. *Bull. Am. Meteorol. Soc.*, 1998, **79**, 61–78.
12. Sinha, H. S. S. and Prakash, S., Electron densities in the equatorial lower ionosphere over Thumba and SHAR. *Adv. Space Res.*, 1996, **18**, 311–318.
13. Strelnikov, B., Rapp, M. and LÄubken, F.-J., A new technique for the analysis of neutral air density fluctuations measured *in situ* in the middle atmosphere. *Geophys. Res. Lett.*, 2003, **30**, 1–5.
14. Sinha, H. S. S., Plasma density irregularities in the equatorial D-region produced by neutral turbulence. *J. Atmos. Terr. Phys.*, 1992, **54**, 49–61.
15. Lübken, F. J., On the extraction of turbulent parameters from atmospheric density fluctuations. *J. Geophys. Res.*, 1992, **97**, 20385–20395.
16. Hill, R. J. and Clifford, S. F., Modified spectrum of atmospheric temperature fluctuations and its application to optical propagation. *J. Opt. Sci. Am.*, 1978, **68**, 892–899.
17. Chen, W. Y., Energy dissipation rates of free atmospheric turbulence. *J. Atmos. Sci.*, 1974, **31**, 2222.
18. Weinstock, J., Energy dissipation rates of turbulence in the stable free atmosphere. *J. Atmos. Sci.*, 1981, **38**, 880–883.
19. Hedin, A. E., Extension of the MSIS thermosphere model into the middle and lower atmosphere. *J. Geophys. Res.*, 1991, **96**, 1159–1172.
20. Fritts, D. C., Bizon, C., Werne, J. A. and Meyer, C. K., Layering accompanying turbulence generation due to shear instability and gravity-wave breaking. *J. Geophys. Res.*, 2003, **108**, 8452.
21. McLandress, C., Alexander, M. J. and Wu, D. L., Microwave limb sounder observations of gravity waves in the stratosphere: A climatology and interpretation. *J. Geophys. Res.*, 2000, **105**, 11947–11967.
22. Lübken, F.-J., Hillert, W., Lehmacher, G. and von Zahn, U., Experiments revealing small impact of turbulence on the energy budget of the mesosphere and the lower thermosphere. *J. Geophys. Res.*, 1993, **98**, 20369–20384.


ACKNOWLEDGEMENTS. We are grateful to Prof. P. Panigrahi, Mr R. N. Misra, Mr M. B. Dadhania and Mr S. B. Banerjee for their help and support. Thanks are also due to the RSR group of VSSC, Thiruvananthapuram for payload integration and necessary launch support. Wavelet software was provided by C. Torrence and G. Compo, and is available at URL: http://paos.colorado.edu/research/wavelets/. This work is supported by Department of Space, Government of India.

Received 23 September 2009; revised accepted 26 May 2010